

Application and adaptation of the truncated Newton method for non-convex plasticity problems.

F. Bormann^a, R.H.J. Peerlings^a, M.G.D. Geers^a

^a*Department of Mechanical Engineering, Eindhoven University of Technology, PO Box 513, 5600 MB Eindhoven, The Netherlands*

Abstract

Small-scale plasticity problems are often characterised by different patterning behaviours ranging from macroscopic down to the atomistic scale. In successful models of such complex behaviour, its origin lies within non-convexity of the governing free energy functional. A common approach to solve such non-convex problems numerically is by regularisation through a viscous formulation. This, however, may require the system to be overdamped and hence potentially has a strong impact on the obtained results. To avoid this side-effect, this paper addresses the treatment of the full non-convexity by an appropriate numerical solution algorithm – the truncated Newton method. The presented method is a double iterative approach which successively generates quadratic approximations of the energy landscape and minimises these by an inner iterative scheme, based on the conjugate gradient method. The inner iterations are terminated when either a sufficient energy decrease is achieved or, to incorporate the treatment of non-convexity, a direction of negative curvature is encountered. If the latter never happens, the method reduces to Newton–Raphson iterations, solved by the conjugate gradient method, with a subsequent line search. However, in the case of a non-convex energy it avoids convergence to a saddle point and adds robustness. The stability of the truncated Newton method is demonstrated for the, highly non-convex, Peierls–Nabarro model, solved within a Finite Element framework. A potential drop in efficiency due to an occasional near singular Hessian is remedied by a trust region like extension, which is physically based on the Peierls–Nabarro disregistry profile. The result is an efficient numerical scheme with a high stability that is independent of any regularisation.

Keywords: Non-convex minimisation, Truncated Newton method, Dislocations, Dislocation pile-ups, Peierls–Nabarro model, Phase boundary,

1. Introduction

Plastic deformation processes in metals are complex phenomena. What may seem to be a homogeneous material behaviour at a macroscopic scale reveals a significant complexity on lower scales. One complexity relates to non-homogeneous plastic slip, attributed to the motion of dislocations and the formation of dislocation patterns [1]. On the atomistic level, dislocations themselves can be seen as a form of patterning: atomistic slip (disregistry) along a glide plane with a high slip gradient in the dislocation core, as assumed in the Peierls-Nabarro (PN) model [2, 3, 4].

On all scales, patterning is associated with a non-convex free energy Ψ . In (strain gradient) crystal plasticity frameworks [1, 5, 6, 7, 8, 9] the non-convexity stems from a latent hardening potential, which is related to the accumulation of trapped dislocations. In models that are based on the mechanics of discrete dislocations or dislocation densities [10, 11, 12, 13, 14], the complex interaction between dislocations or dislocation densities gives rise to non-convexity. On the atomistic scale, continuum models establish the disregistry profile of a dislocation through a periodic, and hence highly non-convex, misfit energy that is intrinsic to the glide plane. A modelling approach that can be adopted for all of the above mentioned scales is given by phase-field modelling [15, 16], which is equally based on a non-convex potential.

For the solution of common non-linear, but convex, energy minimisation problems the Newton-Raphson method presents a suitable and efficient numerical solution method. Based on the gradient and the Hessian of the total free energy it minimises the energy iteratively until its minimiser is found. For non-convex energy minimisation problems, however, it may fail as an indefinite Hessian $\nabla^2\Psi$ evokes convergence towards a saddle point instead of an energy minimum.

One way to deal with the non-convexity is a physical or numerical damping. Adding viscous terms regularises the problem, i.e., it renders the Hessian $\nabla^2\Psi$ positive definite and enables the solution with, e.g., a standard Newton-Raphson scheme. In this respect, two different approaches are commonly followed. i) The non-convex problem is decoupled into a convex elasticity problem and a damped evolution problem of the dislocation (density) configuration. The latter is treated either fully explicitly [10, 17] or partially

implicitly [18]. ii) A damping term is introduced in the non-convex problem and it is solved monolithically with an implicit scheme [8, 19].

The introduction of damping, however, may have a significant impact on the results of evolution problems. Particularly in cases where numerical stability requires overdamping or artificial damping, the obtained results may diverge strongly from the solution of the physical problem. For this reason, rate independent (undamped) problems will be considered here. This requires to deal with the non-convexity in the numerical treatment, as a potentially indefinite Hessian $\nabla^2\Psi$ may lead to the breakdown of conventional solution algorithms such as the Newton-Raphson method.

The objective of this paper is hence a robust numerical solution algorithm for non-convex minimisation problems with a performance independent of any regularisation. As a carrier problem the previously proposed Peierls-Nabarro finite element (PN-FE) model is used [19]. It considers the idealised plane strain case of a finite domain with a single glide plane for edge dislocations. The glide plane is modelled in alignment with the PN model as a zero-thickness interface that splits the domain into two linear elastic regions. Along the glide plane, any relative tangential displacement, or disregistry, induces a misfit energy based on a periodic, and thus non-convex, potential. As a result, the total free energy, which is comprised of a the linear elastic strain energy and the misfit energy, is non-convex. In earlier research, this non-convexity was dealt with using a viscous regularisation [19], which we aim to avoid here.

Methods that are capable of solving non-convex minimisation problems, although conditionally, are for instance the truncated Newton method (also known as line search Newton-conjugate gradient) [20, 21, 22, 23], BFGS [24, 25], the modification of the Hessian to render it positive definite [26, 27], trust region methods [28, 29] or Hessian free methods such as the steepest descent [30] or the non-linear conjugate gradient method [31, 32, 33]. For an overview of these methods the reader is referred to Nocedal and Wright [34].

In this paper, the truncated Newton method is followed. It poses a stable and efficient solution algorithm for general non-convex problems in which the Hessian $\nabla^2\Psi$ is available at reasonable computational cost. A problem-specific trust region like extension increases its stability and efficiency even further. The adapted truncated Newton method minimises Ψ , despite intermittent indefiniteness or near-singularity of $\nabla^2\Psi$, in a straightforward and efficient manner. When close to the minimum, where the energy minimisation problem becomes convex, quadratic convergence behaviour is attained.

This paper is organised as follows. After introducing the non-convex minimisation problem of the PN-FE model in Section 2, the truncated Newton method is summarised and extended by a trust region like approach in Section 3. In Section 4, the stability and efficiency of the proposed algorithm is demonstrated by comparing it with the standard truncated Newton method and the Newton method with line search for a benchmark problem. The paper concludes with a discussion in Section 5.

2. The Peierls-Nabarro finite element model

2.1. Problem statement

The general class of problems considered in this paper is characterised by the two-phase continuum microstructure illustrated in Figure 1. It comprises a soft Phase A that is separated from the harder Phase B by a perfectly and fully coherent phase boundary. Embedded in both phases lies a single glide plane, continuous across the phase boundary. Edge dislocations are introduced into Phase A that move as a result of an externally applied deformation towards the phase boundary, where they pile up. When energetically favourable, dislocation transmission into Phase B takes place.

Notwithstanding the fact that for conciseness the class of problems is limited here to Dirichlet boundary conditions, the derivation for mixed boundary conditions follows a similar approach as outlined below. Equally, an extension towards multiple glide planes or multiple phases is realised straightforwardly.

2.2. Model formulation

Let R^2 be the two-dimensional Euclidean space with the global basis vectors $\{\vec{e}_x, \vec{e}_y\}$ and $\Omega \subset R^2$ the reference configuration of the multi-phase body with outer boundary $\partial\Omega$, consisting of the two phases $\Omega^i \subset \Omega$, $i = \{A, B\}$, with outer boundary $\partial\Omega^i \subset \partial\Omega$ and the internal boundary Γ_{pb} separating both phases. The phase boundary orientation is described by its local basis $\{\vec{e}_{n,\text{pb}}, \vec{e}_{t,\text{pb}}\}$. The vector $\vec{x} \in \Omega$ is the position vector of any material point in Ω and $\vec{u}(\vec{x})$ is the displacement vector at \vec{x} . Assume further that the deformation characterised by $\vec{u}(\vec{x})$ induces a free energy density consisting of the elastic strain energy density ψ_e and the dislocation induced misfit energy ψ_{gp} intrinsic to a single, discrete glide plane. In each Phase i , the glide plane orientation is characterised by the glide plane normal $\vec{e}_{n,\text{gp}}^i$ and the glide direction $\vec{e}_{t,\text{gp}}^i$ which define together the local basis $\{\vec{e}_{t,\text{gp}}^i, \vec{e}_{n,\text{gp}}^i\}$. The vector $\vec{s}^i = s^i \vec{e}_{t,\text{gp}}^i$ denotes the position on glide plane Γ_{gp}^i . In the following,

the superscripts i for the local basis and for the glide plane position will be dropped for conciseness.

Limiting ψ_{gp} to intrinsic glide plane phenomena, the glide plane can be regarded as an internal boundary Γ_{gp}^i splitting Ω^i into two elastic subdomains $\Omega_{\pm}^i \subset \Omega^i$ (see Figure 1). Ω_{+}^i is defined as the subdomain in the direction of $\vec{e}_{n,\text{gp}}^i$ and Ω_{-}^i the other subdomain. The total free energy Ψ of Ω can thus be formulated as

$$\Psi = \int_{\bar{\Omega}} \psi_e \, d\Omega + \int_{\Gamma_{\text{gp}}} \psi_{\text{gp}} \, d\Gamma \quad (1)$$

where $\bar{\Omega} = \Omega \setminus (\Gamma_{\text{gp}} \cup \Gamma_{\text{pb}})$ encompasses all subdomains Ω_{\pm}^i and $\Gamma_{\text{gp}} = \Gamma_{\text{gp}}^A \cup \Gamma_{\text{gp}}^B$.

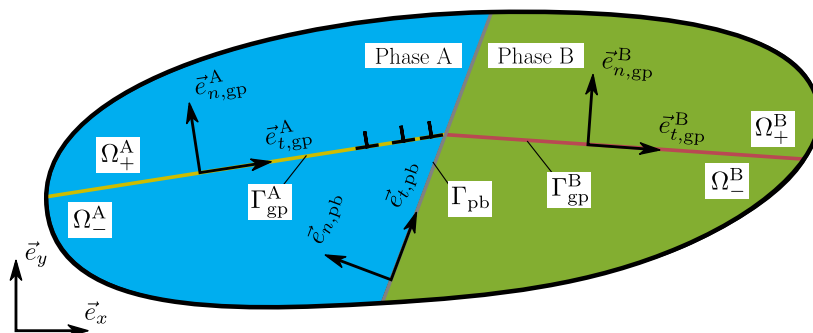


Figure 1: Two-phase microstructure with an internal phase boundary Γ_{pb} and a single glide plane Γ_{gp}^i in each phase.

Under the assumption of linear elasticity, the strain energy density ψ_e in each subdomain Ω_{\pm}^i is defined as

$$\psi_e = \frac{1}{2} \varepsilon_{kl}^e C_{klmn} \varepsilon_{mn}^e \quad (2)$$

under a plane strain condition and with the phase-specific fourth-order elasticity tensor $C_{klmn}(\vec{x}) = C_{klmn}^i$ for $\vec{x} \in \Omega^i$ and the elastic strain tensor

$$\varepsilon_{mn}^e = \frac{1}{2} \left(\frac{\partial u_m}{\partial x_n} + \frac{\partial u_n}{\partial x_m} \right) \quad (3)$$

Correspondingly, the linear elastic stress reads

$$\sigma_{kl} = C_{klmn} \varepsilon_{mn}^e \quad (4)$$

Considering only edge dislocations, the misfit energy ψ_{gp} is given in accordance with the PN model by [2]

$$\psi_{\text{gp}} = \gamma_{us} \sin^2 \left(\frac{\pi \Delta}{b} \right) \quad (5)$$

where γ_{us} is the unstable stacking fault energy and $b = b^i$ the magnitude of the Burgers vector. In this paper, γ_{us} is approximated by conforming it to linear elasticity in the small strain limit [2], which gives

$$\gamma_{us} = \frac{\mu b^2}{2\pi^2 d} \quad (6)$$

with the shear modulus $\mu = \mu^i$ and the interplanar spacing $d = d^i$. The disregistry Δ at glide plane position s is defined as

$$\Delta(s) = \vec{e}_{t,\text{gp}} \cdot (\vec{u}_+ - \vec{u}_-) \quad (7)$$

where \vec{u}^+ and \vec{u}^- represent the displacement vectors of two initially coincident points on Γ_{gp}^i belonging to Ω_+^i and Ω_-^i , respectively. The normal opening of Γ_{gp}^i is constrained to be zero:

$$\vec{e}_{n,\text{gp}} \cdot (\vec{u}_+ - \vec{u}_-) = 0 \quad (8)$$

Along the perfectly bonded phase boundary, displacement and traction continuity are enforced by

$$\vec{u}^{\text{A}} = \vec{u}^{\text{B}} \quad \forall \vec{x} \in \Gamma_{\text{pb}} \quad (9)$$

$$\boldsymbol{\sigma}^{\text{A}} \cdot \vec{e}_{n,\text{pb}} = \boldsymbol{\sigma}^{\text{B}} \cdot \vec{e}_{n,\text{pb}} \quad \forall \vec{x} \in \Gamma_{\text{pb}} \quad (10)$$

On the remote boundary $\partial\Omega$, a displacement field $\vec{u} = \vec{u}_{\text{p}}(\vec{x}, t)$, $\vec{x} \in \partial\Omega$, is introduced to load the domain Ω . The dependency of \vec{u} on the pseudo-time t is used to establish the evolution of the system under a gradually increasing load.

2.3. Finite element discretisation

To determine the equilibrium configuration of Ω under the imposed Dirichlet boundary condition at the discrete time t_n , the total free energy $\Psi(\partial u_k / \partial x_l, \Delta)$ needs to be minimised with respect to $\partial u_k / \partial x_l$ and Δ . For the solution of this minimisation problem, Ω is discretised spatially according to the finite

element method (FEM). The unknown fields $\vec{u}(\vec{x})$ and $\Delta(s)$ are approximated by

$$\vec{u}^h(\vec{x}) = [\vec{e}_x \quad \vec{e}_y] \underline{N}(\vec{x}) \underline{u}, \quad \forall \vec{x} \in \Omega_{\pm}^i \quad (11)$$

$$\Delta^h(s) = \overline{N}(s) \underline{\Delta} \quad \forall \vec{x} \in \Gamma_{\text{gp}}^i \quad (12)$$

where the matrices $\underline{N}(\vec{x})$ and $\overline{N}(s)$ contain the shape functions for Ω_{\pm}^i and Γ_{gp}^i , interpolating the nodal values of \vec{u} and Δ , contained in the column matrices \underline{u} and $\underline{\Delta}$:

$$\underline{N}(\vec{x}) = \begin{bmatrix} N_1(\vec{x}) & 0 & N_2(\vec{x}) & 0 & \cdots \\ 0 & N_1(\vec{x}) & 0 & N_2(\vec{x}) & \cdots \end{bmatrix} \quad (13)$$

$$\overline{N}(s) = [\overline{N}_1(s) \quad \overline{N}_2(s) \quad \cdots] \quad (14)$$

$$\underline{u} = [u_{1,x} \quad u_{1,y} \quad u_{2,x} \quad u_{2,y} \quad \cdots \quad u_{n,x} \quad u_{n,y}]^T \quad (15)$$

$$\underline{\Delta} = [\Delta_1 \quad \Delta_2 \quad \cdots \quad \Delta_n]^T \quad (16)$$

Following Eq. (7), it is possible to express $\underline{\Delta}$ in terms of \underline{u} as

$$\underline{\Delta} = \underline{P} \underline{R} \underline{u} \quad (17)$$

where the rotation matrix \underline{R} projects the displacements \underline{u} , defined in the global basis $\{\vec{e}_x, \vec{e}_y\}$, onto the local basis vector $\vec{e}_{t,\text{gp}}$. \underline{P} is established such that Eq. (7) holds, e.g., for a linear interface element

$$\begin{bmatrix} \Delta^{1-4} \\ \Delta^{2-3} \end{bmatrix} = \begin{bmatrix} -1 & 0 & 0 & 1 \\ 0 & -1 & 1 & 0 \end{bmatrix} \begin{bmatrix} u_{1,t} \\ u_{2,t} \\ u_{3,t} \\ u_{4,t} \end{bmatrix} \quad (18)$$

with points 1 and 2 of Ω_- initially coincident respectively with points 4 and 3 of Ω_+ and $\underline{u}_t = \underline{R} \underline{u}$. Eq. (12) can thus be reformulated in terms of \underline{u} as

$$\Delta^h(s) = \overline{N} \underline{P} \underline{R} \underline{u} \quad (19)$$

Based on Eq. (11), the components of the elastic strain tensor are obtained as

$$\underline{\varepsilon} = [\varepsilon_{xx} \quad \varepsilon_{yy} \quad \gamma_{xy}]^T = \underline{B} \underline{u} \quad (20)$$

with $\gamma_{xy} = 2\varepsilon_{xy}$ and the standard strain-displacement matrix \underline{B}

$$\underline{B} = \begin{bmatrix} \partial N_1/\partial x & 0 & \partial N_2/\partial x & \cdots \\ 0 & \partial N_1/\partial y & 0 & \cdots \\ \partial N_1/\partial y & \partial N_1/\partial x & \partial N_2/\partial y & \cdots \end{bmatrix} \quad (21)$$

Similarly, the disregistry gradient is defined for later use as

$$\frac{d\Delta^h}{ds} = \underline{\bar{B}}\Delta = \underline{\bar{B}}\underline{P}\underline{R}u \quad (22)$$

with

$$\underline{\bar{B}} = [d\bar{N}_1/ds \quad d\bar{N}_2/ds \quad \cdots] \quad (23)$$

By inserting the discretisation as defined above, the total free energy $\Psi(\partial u_k/\partial x_l, \Delta)$ becomes a function of the nodal displacements u :

$$\begin{aligned} \Psi^h(u) &= \int_{\bar{\Omega}} \psi_e^h(u) \, d\Omega + \int_{\Gamma_{gp}} \psi_{gp}^h(u) \, d\Gamma \\ &= \int_{\bar{\Omega}} \frac{1}{2} u^T \underline{B}^T \underline{C} \underline{B} u \, d\Omega + \int_{\Gamma_{gp}} \frac{\mu b^2}{2\pi^2 d} \sin^2 \left(\frac{\pi}{b} \bar{N} \underline{P} \underline{R} u \right) \, d\Gamma \end{aligned} \quad (24)$$

with the Voigt elasticity matrix \underline{C} .

To incorporate the constraint introduced by the Dirichlet boundary conditions at time t_n , the displacement components u can be split into the free (i.e., not prescribed) and prescribed displacements u_f and u_p , respectively, with

$$u = \underline{G}_f u_f + \underline{G}_p u_p \quad (25)$$

Here, \underline{G}_f and \underline{G}_p are the relevant transformation matrices. The minimisation problem hence reduces to finding, for given u_p , the local minimiser u_f^* of Ψ^h for which $\partial \Psi^h / \partial u_f|_{u_f^*} = 0$ and positive definiteness of $\partial^2 \Psi^h / \partial^2 u_f|_{u_f^*}$ holds.

2.4. Conventional Newton-Raphson procedure

The minimisation of Ψ^h poses a nonlinear problem that needs to be solved iteratively. A common way to proceed in solid mechanics is to linearise the stationarity condition $\partial \Psi^h / \partial u_f = 0$ at an initial estimate for the solution and to solve the linearised system to obtain a better estimate. These two steps are repeated until this so-called Newton-Raphson process converges. In

terms of the energy, it implies that, in each iteration i , Ψ^h is approximated by the second-order Taylor expansion around the current estimate \underline{u}_f^i of \underline{u}_f^* :

$$\Psi^h \approx \hat{\Psi}^{i+1} := \Psi^h(\underline{u}_f^i, \underline{u}_p) + \delta \underline{u}_f^T \underline{F}^i + \frac{1}{2} \delta \underline{u}_f^T \underline{K}^i \delta \underline{u}_f \quad (26)$$

with the current gradient $\underline{F}^i = \underline{F}(\underline{u}_f^i)$, the current Hessian $\underline{K}^i = \underline{K}(\underline{u}_f^i)$ and the update $\delta \underline{u}_f = \underline{u}_f^{i+1} - \underline{u}_f^i$. From Eq. (24), the gradient follows as

$$\begin{aligned} \underline{F} = \frac{\partial \Psi^h}{\partial \underline{u}_f} &= \left(\frac{\partial \underline{u}}{\partial \underline{u}_f} \right)^T \frac{\partial \Psi^h}{\partial \underline{u}} = \underline{G}_f^T \int_{\Omega} \underline{B}^T \underline{C} \underline{B} \underline{u} \, d\Omega \\ &\quad + \underline{G}_f^T \int_{\Gamma_{\text{gp}}} \underline{R}^T \underline{P}^T \underline{N}^T T_t \, d\Gamma \end{aligned} \quad (27)$$

with the glide plane shear traction

$$T_t = \frac{\partial \psi_{\text{gp}}}{\partial \Delta} = \frac{\mu b}{2\pi d} \sin \left(\frac{2\pi}{b} \underline{N} \underline{P} \underline{R} \underline{u} \right) \quad (28)$$

Correspondingly, the Hessian reads

$$\begin{aligned} \underline{K} = \frac{\partial^2 \Psi^h}{\partial \underline{u}_f \partial \underline{u}_f} &= \underline{G}_f^T \int_{\Omega} \underline{B}^T \underline{C} \underline{B} \, d\Omega \underline{G}_f \\ &\quad + \underline{G}_f^T \int_{\Gamma_{\text{gp}}} \underline{R}^T \underline{P}^T \underline{N}^T M_{tt} \underline{N} \underline{P} \underline{R} \, d\Gamma \underline{G}_f \end{aligned} \quad (29)$$

with the glide plane stiffness

$$M_{tt} = \frac{\partial^2 \psi_{\text{gp}}}{\partial \Delta^2} = \frac{\mu}{d} \cos \left(\frac{2\pi}{b} \underline{N} \underline{P} \underline{R} \underline{u} \right) \quad (30)$$

As result of the alternating sign of the glide plane stiffness the Hessian \underline{K} may become positive semi-definite, negative semi-definite or indefinite. While the former represents convexity of the quadratic approximation $\hat{\Psi}^{i+1}$, the latter two relate to non-convexity.

Assuming convexity, the update $\delta \underline{u}_f$ is obtained by solving the linear system

$$\frac{\partial \hat{\Psi}^{i+1}}{\partial (\delta \underline{u}_f)} = \underline{F}^i + \underline{K}^i \delta \underline{u}_f = \underline{0} \quad (31)$$

The local minimiser \underline{u}_f^* of Ψ^h (at time t_n) is then found by iteratively solving Eq. (31) and updating the current estimate $\underline{u}_f^{i+1} = \underline{u}_f^i + \delta \underline{u}_f$ until convergence is achieved with $\underline{u}_f^* \approx \underline{u}_f^{\text{conv}} = \underline{u}_f^{i+1}$ – i.e., the common Newton Raphson (NR) method. For the initial estimate \underline{u}_f^1 , two choices are adopted in this paper, as follows. i) Given an update of the pseudo-time t_n , i.e., an incrementally updated constraint \underline{u}_p , the initial estimate is set to $\underline{u}_f^1(t_{k+1}) = \underline{u}_f^{\text{conv}}(t_n)$ with $\underline{u}_f^{\text{conv}}(t_0) = \mathbf{0}$. ii) For the introduction of a dislocation, the converged solution $\underline{u}_f^{\text{conv}}(t_n)$ is perturbed by the approximated displacement field of the new dislocation $\underline{u}_f^{\text{disl}}$. The system is then re-equilibrated with $\underline{u}_f^1(t_n) = \underline{u}_f^{\text{conv}}(t_n) + \underline{u}_f^{\text{disl}}$. A detailed description of the dislocation introduction is given in [19].

In case of non-convexity, the $\delta \underline{u}_f$ obtained by solving (31) does not necessarily indicate the minimum of the quadratic approximation, but possibly a saddle point or even a maximum. Convergence towards \underline{u}_f^* is not guaranteed anymore. Hence, a numerical scheme for non-convex minimisation is required.

3. The truncated Newton method

A suitable numerical method for the non-convex minimisation problem is provided by the family of truncated Newton methods – also known as Newton conjugate gradient methods [34, 20, 21, 22, 23]. They employ a double iterative scheme that finds the approximation of \underline{u}_f^* based on the second-order Taylor expansion (26).

3.1. Outer iterations

In each outer iteration i , the current estimate \underline{u}_f^i is updated by means of a suitable outer search direction \underline{p}^i and step length α^i :

$$\underline{u}_f^{i+1} = \underline{u}_f^i + \delta \underline{u}_f = \underline{u}_f^i + \alpha^i \underline{p}^i \quad (32)$$

The outer search direction \underline{p}^i is determined on the basis of the quadratic potential $\hat{\psi}^{i+1}$ (Eq. (26)) via an iterative scheme, that is outlined in the next section. In case of convexity, \underline{p}^i represents the minimiser of $\hat{\psi}^{i+1}$. With a subsequent line search, that calculates the step length α^i , the potential error of \underline{p}^i with respect to the true non-quadratic energy ψ^h is resolved. In this paper, a backtracking line search algorithm with $0 < \alpha^i \leq 1$ is adopted [34] –

see ahead to Algorithm 3. A suitable step length is reached when the Armijo rule is fulfilled:

$$\Psi^h(\underline{u}_f^i + \alpha^i \underline{p}^i) \leq \Psi^h(\underline{u}_f^i) + c\alpha^i \underline{F}^{iT} \underline{p}^i \quad (33)$$

where the constant $0 < c < 1$ is to be chosen small [34]. For the problem considered here, $c = 10^{-3}$ is used. Numerical experiments showed a negligible influence on the numerical performance for smaller values of c .

The outer iterations of the truncated Newton method terminate with $\underline{u}_f^* \approx \underline{u}_f^{\text{conv}} = \underline{u}_f^{i+1}$ when global convergence is achieved. Hereto, the fulfilment of the following inequalities is required in the present study

$$\|\delta \underline{u}_f\|_\infty \leq \varepsilon_u b \quad (34)$$

$$\|\underline{F}^i\| \leq \varepsilon_f \frac{\mu^A b}{2\pi d} \quad (35)$$

where ε_u and ε_f are the set tolerances. For Sufficient accuracy of the results, tolerances $\varepsilon_u = \varepsilon_f = 10^{-3}$ are used in the simulations. Note that the unit [force/length] of the reference value in the force convergence criterion (35) results from the 2D plane strain formulation.

3.2. Inner iterations

Assuming for now convexity of $\hat{\Psi}^{i+1}$, the truncated Newton method establishes the outer search direction \underline{p}^i by approximately solving the Newton equation Eq. (31) with the conventional conjugate gradient (CG) method [34] as the inner iterative scheme. The CG method constructs \underline{p}^i by successively minimising $\hat{\Psi}^{i+1}$ in search directions \underline{d}_j , $j = 1, 2, 3, \dots$. To avoid confusion with the outer search direction \underline{p}^i , \underline{d}_j is referred to as the inner search direction. As the inner iterations j proceed, an increasingly accurate estimate of \underline{p}^i is obtained by the update $\underline{p}_{j+1}^i = \underline{p}_j^i + \kappa_j \underline{d}_j$ where κ_j is the CG step length

$$\kappa_j = \frac{\underline{r}_j^T \underline{r}_j}{\underline{d}_j^T \underline{K}^i \underline{d}_j} \quad (36)$$

and \underline{r}_j the residual

$$\underline{r}_{j+1} = \underline{r}_j - \kappa_j \underline{K}^i \underline{d}_j = -\underline{F}^i - \underline{K}^i \underline{p}_{j+1}^i \quad (37)$$

The CG method's main feature – and the reason for its numerical efficiency – is the property that all \underline{d}_j are conjugate to each other, leading to a fast decrease of \underline{r}_j .

The inner iterations are terminated with $\underline{p}^i = \underline{p}_j^i$ when a termination criterion is met. Hereto, Nash and Sofer [20] proposed a test based on the pseudo-potential (cf. (26))

$$Q_j = \underline{p}_j^{iT} \underline{F}^i + \frac{1}{2} \underline{p}_j^{iT} \underline{K}^i \underline{p}_j^i \quad (38)$$

It is suggested to terminate the CG iterations when

$$\frac{(Q_j - Q_{j-1})}{Q_j/j} \leq \eta^i \quad (39)$$

where $\eta^i \in [0, 1)$ is the set tolerance. A numerically efficient manner to update Q_j was derived by Fasano and Roma [23] as follows

$$Q_j = Q_{j-1} + \left(\frac{1}{2} \text{sgn}(\underline{d}_j^T \underline{K}^i \underline{d}_j) - 1 \right) \frac{\underline{r}_j^T \underline{r}_j}{|\underline{d}_j^T \underline{K}^i \underline{d}_j|} \quad (40)$$

Ideally, the tolerance η^i is chosen adaptively to ensure a loose tolerance distant from the local minimiser u_f^* and a tight tolerance in the proximity of the minimiser u_f^* . In this context, Eisenstat and Walker [35] proposed

$$\eta^{i+1} = \frac{\|\underline{F}^{i+1} - \underline{F}^i - \alpha^i \underline{K}^i \underline{p}^i\|}{\|\underline{F}^i\|} \quad (41)$$

with $\eta^1 \in [0, 1)$. Additionally, safeguards are required for a smooth performance of the solution algorithm. A first safeguard prevents a premature small tolerance due to a small step size or a coincidental good agreement between the Ψ^h and its quadratic approximation $\hat{\Psi}^{i+1}$. It requires the pending tolerance η^{i+1} to be no less than $(\eta^i)^\zeta$ if the latter is larger than the set threshold $\theta \in [0, 1)$. The safeguard thus reads

$$\eta^{i+1} \leftarrow \max(\eta^{i+1}, (\eta^i)^\zeta) \quad \text{if } (\eta^i)^\zeta > \theta \quad (42)$$

Eisenstat and Walker [35] proposed $\zeta = (1 + \sqrt{5})/2$ based on a convergence of r-order [36] $(1 + \sqrt{5})/2$ under the assumption of an initial guess u_f^1 sufficiently close to u_f^* . This, however, does not hold for the problem considered here; numerical experiments showed that the computational efficiency is strongly increased for $\zeta = 1.25$. As a second safeguard, an upper bound η_u and a lower bound η_l are introduced to prevent too loose tolerances and over-solving:

$$\eta^{i+1} \leftarrow \max(\min(\eta^{i+1}, \eta_u), \eta_l) \quad (43)$$

3.3. Truncation

3.3.1. Curvature criterion

To address the potential non-convexity of $\hat{\Psi}^{i+1}$, the truncated Newton method extends the standard CG method by the nonpositive curvature test

$$\underline{d}_j^T \underline{K}^i \underline{d}_j \leq 0 \quad (44)$$

As soon as an inner search direction \underline{d}_j meets this criterion, i.e., it points into a direction of negative curvature within Q^i , the inner iterations are terminated with $\underline{p}^i = \underline{p}_j^i$, avoiding the direction with negative curvature. The algorithm then proceeds with the backtracking line search, followed by the construction of a new quadratic approximation in a next outer iteration – see Section 3.1.

3.3.2. Disregistry criterion

Solely criterion (44), does not necessarily guarantee computational efficiency, as Nocedal and Wright [34] pointed out: a near singular Hessian \underline{K}^i may yield a long and poor outer search direction \underline{p}^i , leading to a computationally expensive line search with only a small reduction of Ψ^h .

To prevent this from occurring, an extension of the standard truncated Newton method is proposed by an additional trust region like truncation criterion, as follows. Considering the Peierls-Nabarro dislocation, a strict monotonicity of the disregistry profile is present within the core region: $d\Delta/ds < 0$ for a positive edge dislocation and $d\Delta/ds > 0$ for a negative edge dislocation. This is illustrated in Figure 2, which sketches the analytical solution of the disregistry profile for a positive PN edge dislocation in an infinite homogeneous medium [2]. This requirement leads, using Eq. (22), to the following additional criterion. If for any position s the inequality

$$\text{sgn}(\overline{B} \underline{P} \underline{R}(u^i + \underline{G}_f \underline{p}_{j+1}^i)) \neq \text{sgn}(\overline{B} \underline{P} \underline{R}u^i) \quad (45)$$

yields, i.e., the updated inner search direction \underline{p}_{j+1}^i leads to a change of the sign of the disregistry gradient, presuming a step length of $\alpha^i = 1$, the inner iteration is truncated with $\underline{p}^i = \underline{p}_j^i$. This criterion is generally violated as a result of the near singularity of \underline{K} , which arises through a negative glide plane contribution (cf. Eq. (29)). Thus, for computational efficiency, the disregistry criterion is checked only in a region r_Δ around each dislocation, as shown in Figure 2 for a positive dislocation. r_Δ is determined as the region in which $M_{tt} < 0$, i.e., $b/4 \leq \Delta \leq 3b/4$, extended by a small distance

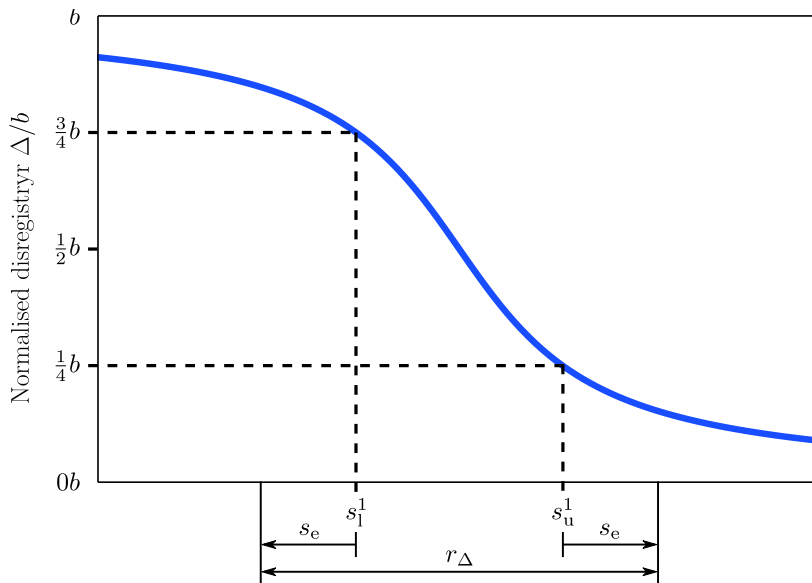


Figure 2: Sketch of the analytical solution for the disregistry profile of a positive PN edge dislocation in an infinite homogeneous medium. r_Δ defines the region in which the disregistry termination criterion is applied.

s_e . In this paper $s_e = b$ is chosen. Numerical experiments showed that a small increase or reduction of s_e has a negligible influence on the numerical performance.

3.4. The overall incremental-iterative algorithm

With this additional criterion, one has to be aware of the impact of the boundary constraints \underline{u}_p applied on $\partial\Omega$. Following Eq. (27), an incremental update of \underline{u}_p induces a rather strong gradient (residual) \underline{F}^i ($-r_1$) concentrated on the nodes adjacent to $\partial\Omega$. With an increasing number of inner iterations j , the residuals r_j spread iteratively inwards into the bulk Ω . In this context, high residuals can emerge at the glide plane and invoke premature termination due to criterion (45). It is thus essential to split at each pseudo-time t_n the solution process into two steps. The first step freezes the current disregistry profile along the glide plane Γ_{gp} with $\delta\Delta = 0$ and assesses the elastic response emanating from \underline{u}_p . It comprises a purely convex minimisation and requires therefore only a single outer iteration i using a tight tolerance η_{ini} . In the second step the complete non-convex energy is iteratively minimised until global convergence is attained.

The main algorithm of the truncated Newton method, executed at each pseudo-time t_n , is outlined in Algorithm 1 with the Sub-algorithms 2 and 3.

Algorithm 1 The adapted truncated Newton method

- 1: Set tolerances ε_u , ε_f , η_{ini} , η_u and η_l
 - 2: Initialisation of u_p , u_f^1 and gradient F^1
 - 3: **for** $i = 1, 2, 3, \dots$ **do**
 - 4: **if** $i = 1$ **then**
 - 5: Constrain disregistry profile with $\delta\Delta = 0$
 - 6: Set tolerance $\eta^1 = \eta_{\text{ini}}$
 - 7: **else**
 - 8: Lift disregistry constraint
 - 9: Set tolerance η^i using Eq. (41)-(43) and $\eta^2 = \eta_u$
 - 10: Calculate Hessian K^i
 - 11: Calculate p^i using function Inner Loop (Algorithm 2)
 - 12: Calculate α^i using function Backtracking Line Search (Algorithm 3)
 - 13: Set $u_f^{i+1} = u_f^i + \alpha^i p^i$
 - 14: Update gradient F^{i+1}
 - 15: Convergence test using Eq. (34) and (35)
 - 16: **if** Convergence **then exit** with $u_f^* \approx u_f^{i+1}$
-

4. Comparative performance study

4.1. Problem statement

To demonstrate the stability of the truncated Newton method and the added value of the trust region like extension, the two-phase continuum microstructure illustrated in Figure 3 is considered. It comprises a soft Phase A that is flanked by the harder Phase B. The single glide plane $\Gamma_{gp}^{A/B}$ lies perpendicular to and continuous across the perfectly bonded phase boundary. The local bases of glide plane and phase boundary are thus in alignment with the global basis: $\vec{e}_{t,gp} = \vec{e}_x$, $\vec{e}_{n,gp} = \vec{e}_y$ and $\vec{e}_{n,pb} = \vec{e}_x$. On the outer boundary $\partial\Omega$ a shear deformation is introduced that corresponds to a constant shear stress $\tau = \bar{\tau}t$ for a purely linear elastic medium, i.e., without glide plane. Here, $\bar{\tau} = 0.19 \cdot (\mu^A b / 2\pi d)$ is the target shear load and $t \in [0, 1]$ the pseudo-time. Four discrete time points $t_n = n/4$ are considered to simulate the build-up of a four-dislocation pile-up under the incrementally increasing

Algorithm 2 Inner loop of the adapted truncated Newton method

```
1: function INNER LOOP
2:   Set  $r_1 = -\underline{F}^i$ ,  $d_1 = r_1$ ,  $\underline{p}_1^i = 0$  and  $Q_0 = 0$ 
3:   for  $j = 1, 2, 3, \dots$  do
4:     if  $d_j^T \underline{K}^i d_j \leq 0$  then
5:       if  $j = 1$  then
6:         return  $\underline{p}^i = -\underline{F}^i$ 
7:       else
8:         return  $\underline{p}^i = \underline{p}_j^i$ 
9:        $\kappa_j = r_j^T r_j / d_j^T \underline{K}^i d_j$ 
10:       $\underline{p}_j^i = \underline{p}_j^i + \kappa_j d_j$ 
11:      if  $\text{sgn}(\overline{BPR}(u_f^i + \underline{p}_j^i)) \neq \text{sgn}(\overline{BPR}u_f^i)$  then
12:        if  $j = 1$  then
13:          return  $\underline{p}^i = -\underline{F}^i$ 
14:        else
15:          return  $\underline{p}^i = \underline{p}_j^i$ 
16:       $r_{j+1} = r_j - \kappa_j \underline{K}^i d_j$ 
17:       $Q_j = Q_{j-1} - \frac{1}{2}(r_j^T r_j)^2 / d_j^T \underline{K}^i d_j$ 
18:      if  $j(Q_j - Q_{j-1})/Q_j \leq \eta^i$  then
19:        return  $\underline{p}^i = \underline{p}_j^i$ 
20:       $\beta_{j+1} = r_{j+1}^T r_{j+1} / r_j^T r_j$ 
21:       $d_{j+1} = r_{j+1} + \beta_{j+1} d_j$ 
```

Algorithm 3 Backtracking Line Search of the truncated Newton Method

```
1: function BACKTRACKING LINE SEARCH
2:   Set  $\alpha = 1$ ,  $\rho \in (0, 1)$ ,  $c \in (0, 1)$ 
3:   repeat
4:      $\alpha = \rho \alpha$ 
5:     until  $\Psi^h(u_f^i + \alpha^i \underline{p}^i) \leq \Psi^h(u_f^i) + c \alpha^i \underline{F}^{iT} \underline{p}^i$ 
6:   return  $\alpha^i = \alpha$ 
```

shear deformation. At each time t_n , the respective minimisation problem is solved first in sub-increment a. Subsequently, a Peierls-Nabarro dislocation dipole, centred in Phase A, is introduced and the system is re-equilibrated in sub-increment b. As a result the newly introduced dislocation moves towards the phase boundary and the pile-up process evolves.

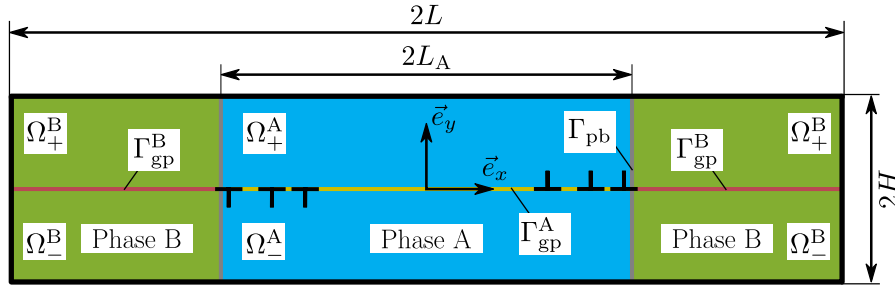


Figure 3: Two-phase microstructure with a single glide plane perpendicular to the phase boundaries.

Intrinsic to this problem is a symmetry with respect to the model centre ($\vec{x} = \vec{0}$) which is characterised by $\vec{u}(-\vec{x}) = -\vec{u}(\vec{x})$. It hence suffices to consider half of the model domain, $0 \leq x \leq L$, and to enforce this symmetry condition along $x = 0$ by means of standard FEM tie constraints. For the discretisation linear triangular elements with one central Gauss point for Ω_{\pm}^i and linear interface elements with two Gauss points for Γ_{gp}^i are used. A convergence study showed a good accuracy in capturing dislocation behaviour for element sizes of $h_{max} = b/8$ in the vicinity of the phase boundary. Away from the region of interest, however, the mesh can be rapidly coarsened. The resulting discretisation is displayed in Figure 4. It has a total of 482288 bulk elements and 770 interface elements. The adopted model parameters are listed in Table 1.

To show the benefits of the truncated Newton method, simulations are carried out with the following numerical solution algorithms: i) the Newton–Raphson method, solved by CG, with line search, ii) the standard truncated Newton method which uses only the conventional truncation criterion (44), and iii) the adapted truncated Newton method which in addition uses the problem specific truncation criterion (45). All algorithms have been implemented within an in-house code for the quantitative comparison. The numerical parameters employed are listed in Table 2.

Parameters	Explanation	Value
$2H$	Model height	$500b$
$2L$	Model width	$1000b$
$2L_A$	Width of Phase A	$500b$
h_{max}	Maximum element size in refined region	$b/8$
μ^B/μ^A	Phase contrast	1.75

Table 1: Model parameters; see Figure 3 for the definition of the geometry parameters

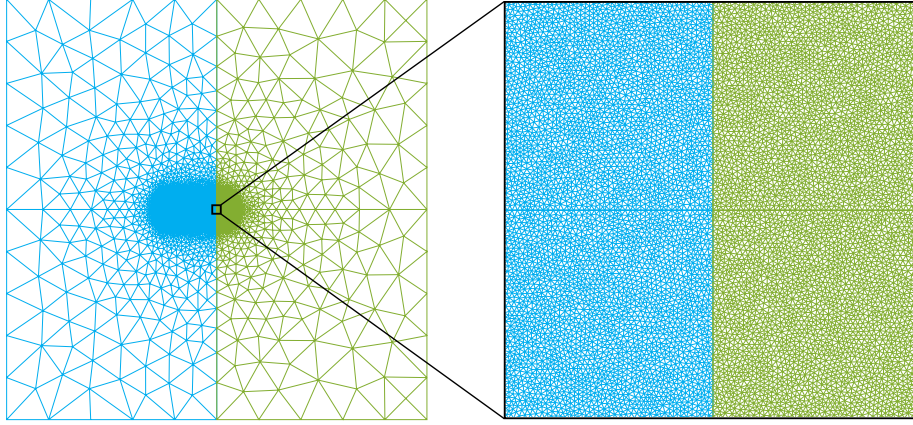


Figure 4: Discretised model for the two-phase microstructure.

Parameters	Description	Value
ε_u	Displacement tolerance for outer loop	$1 \cdot 10^{-3}$
ε_f	Force tolerance for outer loop	$1 \cdot 10^{-3}$
θ	Threshold for safeguard of η^i	$5 \cdot 10^{-2}$
ζ	Exponent for safeguard of η^i	1.25
η_l	Lower bound for tolerance of inner loop	$5 \cdot 10^{-3}$
η_u	Upper bound for tolerance of inner loop	$1 \cdot 10^{-1}$
η_{ini}	Tolerance of inner loop for first outer iteration	$1 \cdot 10^{-4}$
s_e	Cut-off radius for additional termination criterion	b
ρ	Reduction factor for line search	0.75
c	Gradient factor for Armijo condition	$1 \cdot 10^{-3}$

Table 2: Numerical parameters used in the performance assessment

4.2. Simulation results

The simulation results of the PN-FE model are illustrated in Figure 5. It shows the build-up of the 4-dislocation pile-up at the discrete times t_n and sub-increments a (before dislocation nucleation) and b (after dislocation nucleation). The results illustrate the successive compression of the existing part of the pile-up and the addition of a new dislocation to it with each new level of applied deformation. The left column visualises the dislocation evolution in terms of stress-field σ_{xx} for the close-up view $L_A - 140b \leq x \leq L_A + 10b$ and $-20b \leq y \leq 20b$. The dashed line indicates the position of the phase boundary at $x = L_A$. A more detailed insight into the local dislocation structure of the evolving pile-up is given in the right column by the disregistry profile Δ . Here, the grey area indicates the location of Phase B. Dislocations are located at positions s where $\Delta = (j - 1/2)b$, $j = 1, 2, 3, 4$.

4.3. Solver comparison

For the Newton–Raphson method with line search, the missing capability for non-convex minimisation triggers an instability. Convergence is only ensured for sub-increment a at time t_1 , where no dislocation is present and the problem thus is convex. As soon as a dislocation is introduced (in sub-increment b) the problem is rendered non-convex and the algorithm fails convergence: Starting in outer iteration $i = 47$, the non positive definite Hessian leads to a search direction \underline{p}^i for which a sufficient energy decrease requires an extensive line search. As a result, the update $\delta \underline{u}$ is negligibly small and the estimate \underline{u}^i stays in the non-convex region. This is illustrated in Figure 6 by the disregistry profiles $\Delta(\underline{u}_f^i + \underline{p}^i)$ (Figure 6a) and $\Delta(\underline{u}_f^i + \alpha^i \underline{p}^i)$ (Figure 6b) in comparison with $\Delta(\underline{u}_f^i)$. Simulations showed that for the conventional Newton–Raphson method (without line search) the solution diverges as a result of the poor search direction, and fails equally in convergence.

Both truncated Newton methods, on the contrary, converge at all times t_n . To compare both approaches, at each sub-increment of all t_n the elapsed wall times of the inner iterations and the line search iterations are registered. The results are presented in Figure 7, with the inner iterations and line search iterations represented by the light and dark colour bar, respectively. For each method, the major part of the CPU time is spent in the inner iterations ($\approx 90\%$). The comparison of both methods demonstrates the improved performance of the adapted truncated Newton method – it beats the standard method by roughly a factor of 1.5 in most sub-increments.

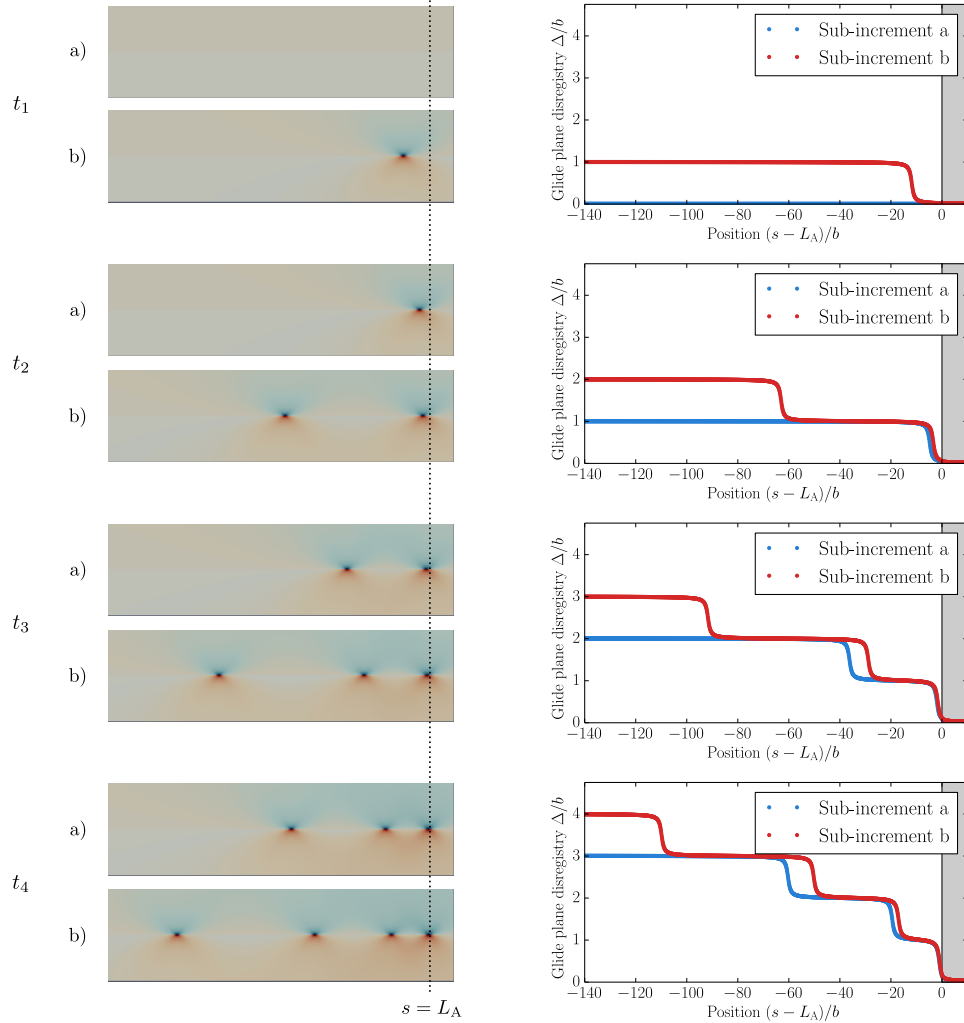


Figure 5: Build-up of a 4-dislocation pile-up at the discrete times $t_n = n/4$ and sub-increments a (before dislocation nucleation) and b (after dislocation nucleation). Left: Close-up view of the qualitative stress-field σ_{xx} ; the dashed line indicates the phase boundary. Right: Disregistry profile along the glide plane; the grey area illustrates the position of Phase B.

The origin of the differences in wall time lies within the occasional near singularity of the Hessian \underline{K}^i as stated before. Despite the termination due to negative curvature, the near singularity yields sometimes a search direction \underline{p}^i of poor quality. Such an occurrence is illustrated in Figure 8, in terms of the disregistry profiles $\Delta(\underline{u}_f^i + \underline{p}^i)$ in Figure 8a) and $\Delta(\underline{u}_f^i + \alpha^i \underline{p}^i)$ in Figure 8b) in comparison with $\Delta(\underline{u}_f^i)$, in iteration $i = 3$ of sub-increment b of time step t_3 . After acquiring a poor search direction \underline{p}^i , the subsequent backtracking line search needs to perform a large number of iterations until the Armijo rule is met and a well-posed disregistry profile with a non-negligible update $\delta \underline{u}$ is recovered. The adapted truncated Newton method, on the contrary, not only prevents an extensive line search, it also reduces the computational expense of the inner loop by avoiding the (inner) iteratively increasing error of \underline{p}^i .

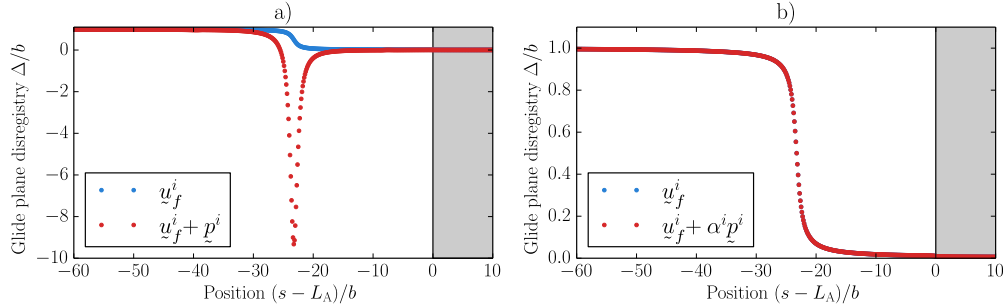


Figure 6: Disregistry profile for the Newton–Raphson method with line search as a result of near singular Hessian \underline{K}^i at time t_1 and sub-increment b (after dislocation nucleation) for $i = 47$: (a) $\Delta(\underline{u}_f^i + \underline{p}^i)$, i.e., without line search; (b) $\Delta(\underline{u}_f^i + \alpha^i \underline{p}^i)$, i.e., with line search.

Such occurrences of poor search directions are accompanied by a slow decrease of the energy Ψ^h . This can be shown by the iterative energy $\Psi^i = \Psi^h(\underline{u}_f^i, \underline{u}_p)$ as a function of the current wall time. Figure 9 illustrates the results for sub-increment b (after dislocation nucleation) at time t_3 in terms of the normalised quantity $\Psi^{i+1}/(\mu^A b^3/2\pi d)$ in Figure 9a) and the relative difference $(\Psi^{i+1} - \Psi_{ref})/\Psi_{ref}$ in Figure 9b). Ψ_{ref} is a reference value and represents the equilibrium energy of a refined simulation ($\varepsilon_u = 10^{-4}$ and $\varepsilon_f = 10^{-6}$). The first plateau observed in the curve for the standard truncated Newton method represents the energy decrease in iteration $i = 3$, in which termination due to negative curvature was recorded. Not only the energy decrease is small, but also the computational cost is rather high due to the

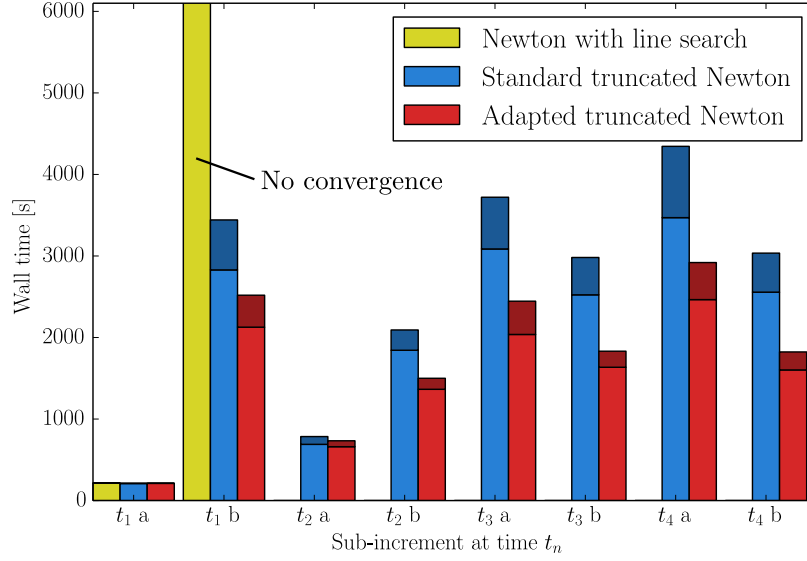


Figure 7: Wall time of the simulation at sub-increments a (before dislocation nucleation) and b (after dislocation nucleation) for each time t_n . Comparison between Newton–Raphson method with line search, standard truncated Newton method and adapted truncated Newton method. Light and dark colour represent inner iterations and line search iterations, respectively.

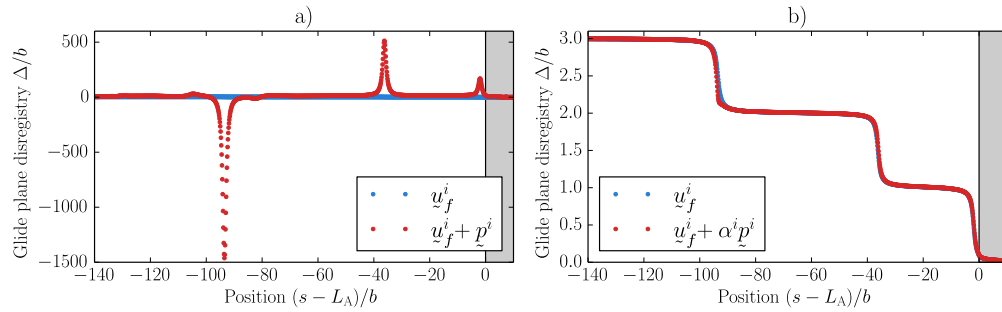


Figure 8: Disregistry profile a) $\Delta(u_f^i + p^i)$ and b) $\Delta(u_f^i + \alpha^i p^i)$ for standard truncated Newton as a result of near singular Hessian \underline{K}^i at time t_3 and sub-increment b (after dislocation nucleation) for $i = 3$.

extensive line search. In the subsequent iterations no negative curvature was recorded. However, occasionally long line searches followed the inner iterations, indicating a poor search direction \underline{p}^i . The adapted truncated Newton method, on the contrary, shows an excellent behaviour throughout as a result of the termination prior to the development of a poor \underline{p}^i . As a consequence, it reaches convergence about 1.5 times faster than the standard truncated Newton method.

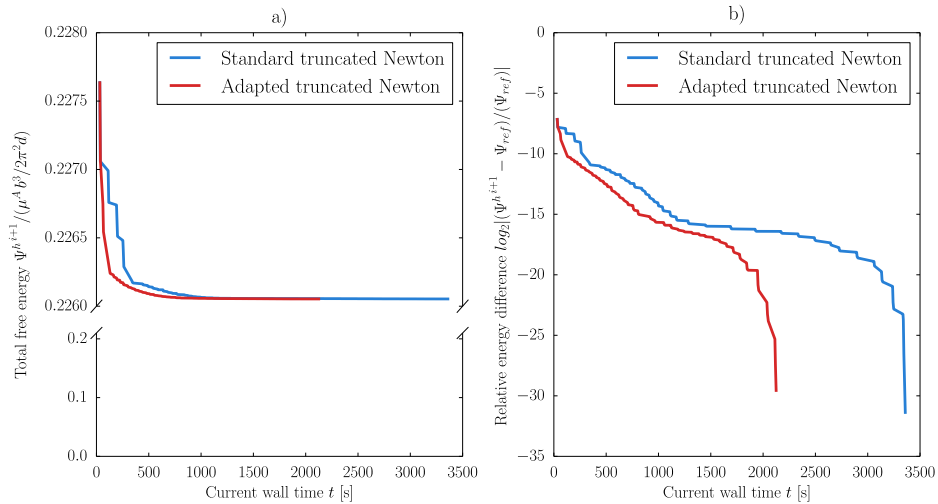


Figure 9: Evolution of the energy of Ψ^h during the iterations in sub-increment b (after dislocation nucleation) at time t_3 as a function of the wall time. Comparison between the standard truncated Newton method and the adapted truncated Newton method: a) the normalised iterative energy and b) the relative iterative energy difference with respect to the reference value Ψ_{ref} obtained from a more accurate simulation.

It can be concluded that the adapted truncated Newton method provides a stable and efficient numerical scheme for the non-convex minimisation problem of the PN-FE model.

5. Conclusion

With the truncated Newton method an adequate numerical solution algorithm for non-convex energy minimisation was presented. By the example of the PN-FE model it was shown that the standard truncated Newton method already provides a stable numerical scheme for non-convex minimi-

sation where the conventional Newton–Raphson method and the Newton–Raphson method with line search fail. Due to its independence of any regularisation, the truncated Newton method is able to provide results that are not negatively affected by, e.g., damping. However, it has also been shown that its efficiency drops occasionally due to a near singular Hessian. A trust region like adaptation, which is based on the Peierls-Nabarro disregistry profile, alleviates this problem and enhances the efficiency approximately by a factor of 1.5. As the performance of the truncated Newton algorithm strongly depends on the specific dislocation behaviour, it can be anticipated that for more complex problems, i.e., larger dislocation pile-ups, the computational gain increases. Although this addition is limited to the presented PN-FE model, it is believed that in other non-convex minimisation problems the underlying physics may provide a solid basis for similar adaptations.

Acknowledgements

We would like to thank Pratheek Shanthraj of the Max Planck Institute for Iron Research for useful comments on the present work. This research is supported by Tata Steel Europe through the Materials innovation institute (M2i) and Netherlands Organisation for Scientific Research (NWO), under the grant number STW 13358 and M2i project number S22.2.1349a.

References

- [1] M. Ortiz, E. Repetto, Nonconvex energy minimization and dislocation structures in ductile single crystals, *Journal of the Mechanics and Physics of Solids* 47 (1999) 397–462.
- [2] J. Hirth, J. Lothe, *Theory of Dislocations*, Wiley, New York, 1982.
- [3] B. Joós, Q. Ren, M. Duesbery, Peierls-Nabarro model of dislocations in silicon with generalized stacking-fault restoring forces, *Physical Review B* 50 (1994) 5890–5898.
- [4] G. Schoeck, The core structure, recombination energy and Peierls energy for dislocations in Al, *Philosophical Magazine A* 81 (2001) 1161–1176.
- [5] D. Kochmann, K. Hackl, The evolution of laminates in finite crystal plasticity: a variational approach, *Continuum Mechanics and Thermodynamics* 23 (2011) 63–85.

- [6] C. Miehe, M. Lambrecht, E. Gürses, Analysis of material instabilities in inelastic solids by incremental energy minimization and relaxation methods: Evolving deformation microstructures in finite plasticity, *Journal of the Mechanics and Physics of Solids* 52 (2004) 2725–2769.
- [7] K. Hackl, D. Kochmann, Relaxed potentials and evolution equations for inelastic microstructures, *IUTAM Symposium on Theoretical, Computational and Modelling Aspects of Inelastic Media* 11 (2008) 27–39.
- [8] T. Yalcinkaya, W. Brekelmans, M. Geers, Deformation patterning driven by rate dependent non-convex strain gradient plasticity, *Journal of the Mechanics and Physics of Solids* 59 (2011) 1–17.
- [9] B. Klusemann, T. Yalçinkaya, M. Geers, B. Svendsen, Application of non-convex rate dependent gradient plasticity to the modeling and simulation of inelastic microstructure development and inhomogeneous material behavior, *Computational Materials Science* 80 (2013) 51–60.
- [10] E. Van der Giessen, A. Needleman, Discrete dislocation plasticity: a simple planar model, *Modelling and Simulation in Materials Science and Engineering* 3 (1995) 689–735.
- [11] A. Vattré, B. Devincere, F. Feyel, R. Gatti, S. Groh, O. Jamond, A. Roos, Modelling crystal plasticity by 3D dislocation dynamics and the finite element method: the discrete-continuous model revisited, *Journal of the Mechanics and Physics of Solids* 63 (2014) 491–505.
- [12] A. Acharya, A model of crystal plasticity based on the theory of continuously distributed dislocations, *Journal of the Mechanics and Physics of Solids* 49 (2001) 761–784.
- [13] C. Fressengeas, V. Taupin, L. Capolungo, An elasto-plastic theory of dislocation and disclination fields, *International Journal of Solids and Structures* 48 (2011) 3499–3509.
- [14] T. Hochrainer, S. Sandfeld, M. Zaiser, P. Gumbsch, Continuum dislocation dynamics: towards a physical theory of crystal plasticity, *Journal of the Mechanics and Physics of Solids* 63 (2014) 167–178.
- [15] Y. Wang, J. Li, Phase field modeling of defects and deformation, *Acta Materialia* 58 (2010) 1212–1235.

- [16] J. Mianroodi, A. Hunter, I. Beyerlein, B. Svendsen, Theoretical and computational comparison of models for dislocation dissociation and stacking fault/core formation in fcc crystals, *Journal of the Mechanics and Physics of Solids* 95 (2016) 719–741.
- [17] S. Sandfeld, T. Hochrainer, P. Gumbsch, M. Zaiser, Numerical implementation of a 3D continuum theory of dislocation dynamics and application to micro-bending, *Philosophical Magazine* 90 (2010) 3697–3728.
- [18] X. Zhang, A. Acharya, N. Walkington, J. Bielak, A single theory for some quasi-static, supersonic, atomic, and tectonic scale applications of dislocations, *Journal of the Mechanics and Physics of Solids* 84 (2015) 145–195.
- [19] F. Bormann, R. Peerlings, M. Geers, B. Svendsen, A computational approach towards modelling dislocation transmission across phase boundaries, Submitted, arXiv:1810.08052 [cond-mat.mtrl-sci].
- [20] S. Nash, A. Sofer, Assessing a search direction within a truncated-Newton method, *Operations Research Letters* 9 (1990) 219–221.
- [21] D. Xie, T. Schlick, Efficient implementation of the truncated-Newton algorithm for large-scale chemistry applications, *SIAM Journal on Optimization* 10 (1999) 132–154.
- [22] S. Nash, A survey of truncated-Newton methods, *Journal of Computational and Applied Mathematics* 124 (2000) 45–59.
- [23] G. Fasano, M. Roma, Preconditioning Newton-Krylov methods in non-convex large scale optimization, *Computational Optimization and Applications* 56 (2013) 253–290.
- [24] D.-H. Li, M. Fukushima, A modified BFGS method and its global convergence in nonconvex minimization, *Journal of Computational and Applied Mathematics* 129 (2001) 15–35.
- [25] G. Yuan, Z. Sheng, B. Wang, W. Hu, C. Li, The global convergence of a modified BFGS method for nonconvex functions, *Journal of Computational and Applied Mathematics* 327 (2018) 274–294.

- [26] R. Schnabel, E. Eskow, A revised modified Cholesky factorization algorithm, *SIAM Journal on Optimization* 9 (1999) 1135–1148.
- [27] C. Kelley, L.-Z. Liao, Explicit pseudo-transient continuation, *Pacific Journal of Optimization* 9 (2013) 77–91.
- [28] R. Byrd, R. Schnabel, G. Shultz, A trust region algorithm for nonlinearly constrained optimization, *SIAM Journal on Numerical Analysis* 24 (1987) 1152–1170.
- [29] A. Conn, N. Gould, P. Toint, *Trust Region Methods*, SIAM, 2000.
- [30] H. Akaike, On a successive transformation of probability distribution and its application to the analysis of the optimum gradient method, *Annals of the Institute of Statistical Mathematics* 11 (1959) 1–16.
- [31] Z. Wei, G. Li, L. Qi, Global convergence of the Polak-Ribière-Polyak conjugate gradient method with an Armijo-type inexact line search for nonconvex unconstrained optimization problems, *Mathematics of Computation* 77 (2008) 2173–2193.
- [32] G. Yuan, Z. Wei, Q. Zhao, A modified Polak–Ribière–Polyak conjugate gradient algorithm for large-scale optimization problems, *IIE Transactions* 46 (2014) 397–413.
- [33] M. Sun, J. Liu, Three modified Polak-Ribière-Polyak conjugate gradient methods with sufficient descent property, *Journal of Inequalities and Applications* 2015 (2015) 125.
- [34] J. Nocedal, S. Wright, *Numerical Optimization*, Springer Science+Business Media, LLC, 2006.
- [35] S. Eisenstat, H. Walker, Choosing the forcing terms in an inexact Newton method, *SIAM Journal on Scientific Computing* 17 (1996) 16–32.
- [36] J. M. Ortega, W. C. Rheinboldt, 9. Rates of convergence--general, in: *Iterative Solution of Nonlinear Equations in Several Variables*, Society for Industrial and Applied Mathematics, 2000, pp. 281–298.